Article

Universal Method for the Fabrication of Detachable Ultrathin Films of Several Transition Metal Oxides

Sherdeep Singh, Miguel Festin, Warren R. T. Barden, Luan Xi, James T. Francis, and Peter Kruse

ACS Nano, **2008**, 2 (11), 2363-2373 • Publication Date (Web): 30 October 2008

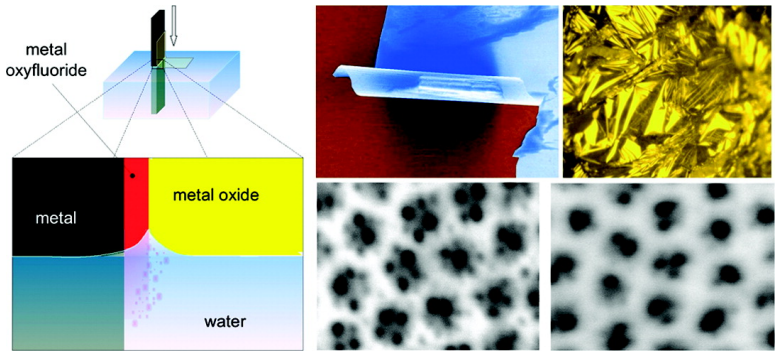

More About This Article

Additional resources and features associated with this article are available within the HTML version:

- Supporting Information
- Access to high resolution figures
- Links to articles and content related to this article
- Copyright permission to reproduce figures and/or text from this article

View the Full Text HTML

Universal Method for the Fabrication of Detachable Ultrathin Films of Several Transition Metal Oxides

Sherdeep Singh,[†] Miguel Festin,[†] Warren R. T. Barden,[†] Luan Xi,[‡] James T. Francis,[‡] and Peter Kruse[†,*]

[†]Department of Chemistry, McMaster University, 1280 Main Street W, Hamilton, Ontario L8S 4M1, Canada, and [‡]Surface Science Western, Western Science Center, University of Western Ontario, London, Ontario N6A 5B7, Canada

ABSTRACT Ultrathin films are important nanoscale structures that are used extensively in a variety of technological contexts. However, it has traditionally been difficult and costly to fabricate detachable and purely inorganic high aspect ratio films with controlled thickness and good uniformity. Here we report a versatile method to make separable purely inorganic membranes of various metal oxides such as Nb_2O_5, TiO_2, WO_3, and Ta_2O_5 with thicknesses ranging from 30 to 150 nm. Fluoride ions are migrated through the oxide film and upon arrival at the oxide—metal interface form a sacrificial soluble oxyfluoride layer. Fluorine also plays a role in controlling the porosity of the films. The study exposes the mechanism behind the detachment process that is largely due to the fast migration of fluoride anions relative to oxygen anions. The resulting films have a wide range of potential applications as catalysts or catalyst supports, filtration membranes, sensors, and more.

KEYWORDS: porosity · detachable · anodization · thin membranes · ion migration · etching · metal oxides

Ultrathin films have been key to numerous technological advances in microelectronics, optics, fuel cells, filtration, protective coatings, catalysts, and sensing devices.[1−4] Several well-established techniques such as chemical vapor deposition, reactive sputtering,[5,6] reactive ion plating,[7] and pulsed laser-assisted evaporation[8] are available to form thin films of a variety of materials. The drawback is that the films are strongly adherent to the surface and cannot be detached as free-standing membranes for uses in separation of gases, filtration of macromolecules, sheet actuators, catalyst surfaces, and nanolithographic templates.

Free-standing ultrathin organic/inorganic hybrid films have recently gained popularity.[9−11] Poor thermal stability and lack of purity, however, have limited their use to specific environmental conditions and have led to an interest in the fabrication of purely inorganic thin films which are robust and stable under harsh conditions. Fabrication methods based on photolithography, sol−gel techniques, and surfactant-assisted templating have recently shown a lot of promise for the fabrication of free-standing, purely inorganic and ultrathin films of Si, Pt, Fe, C, and CdSe.[3,12,13] Interest in the creation of flexible electronics based on thin, crystalline semiconductor ribbons has led to the creative use of anisotropic etching,[14] silicon-on-insulator structures,[15] self-folding structures,[16] and strained layers on etchant-sensitive substrates, which form wrinkled membranes upon release.[17,18] Linked carbon layers produced by wet-chemical methods have also recently been reported.[19] Despite these advances, each method is usually limited to a particular material, leaving room for the development of additional processes suitable for complementary materials. In the case of semiconductors (GaN[20,21] and Si[22]), sacrificial layers have been deposited before the thin film was grown. Later, the sacrificial layer can be dissolved to yield a free-standing film. A different variation of the sacrificial layer trick has been applied by us previously during anodic formation of tantalum oxide.[23]

Anodic oxidation of metal substrates in appropriate electrolyte solutions is an easy, fast, and energy-efficient technique for growing metal oxide films with well-defined thickness and porosity.[24−27] However, these films are adherent to the substrate surface and are not easily separable, limiting their potential applications. Previously, we reported a simple method for the fabrication of fully detachable, ultrathin (35−100 nm thickness), and uniformly porous tantalum oxide membranes.[23] We found that the relatively fast migration of fluoride ions compared to other ions (such as O^{2-}), a phenomenon also studied by Shimizu and co-workers,[28,29] led to the facile film detachment. A thin oxyfluoride layer at the metal/metal−oxide interface acts as

*Address correspondence to pkruse@mcmaster.ca.

Received for review August 1, 2008 and accepted October 14, 2008.

Published online October 30, 2008.
10.1021/nn800488h CCC: $40.75

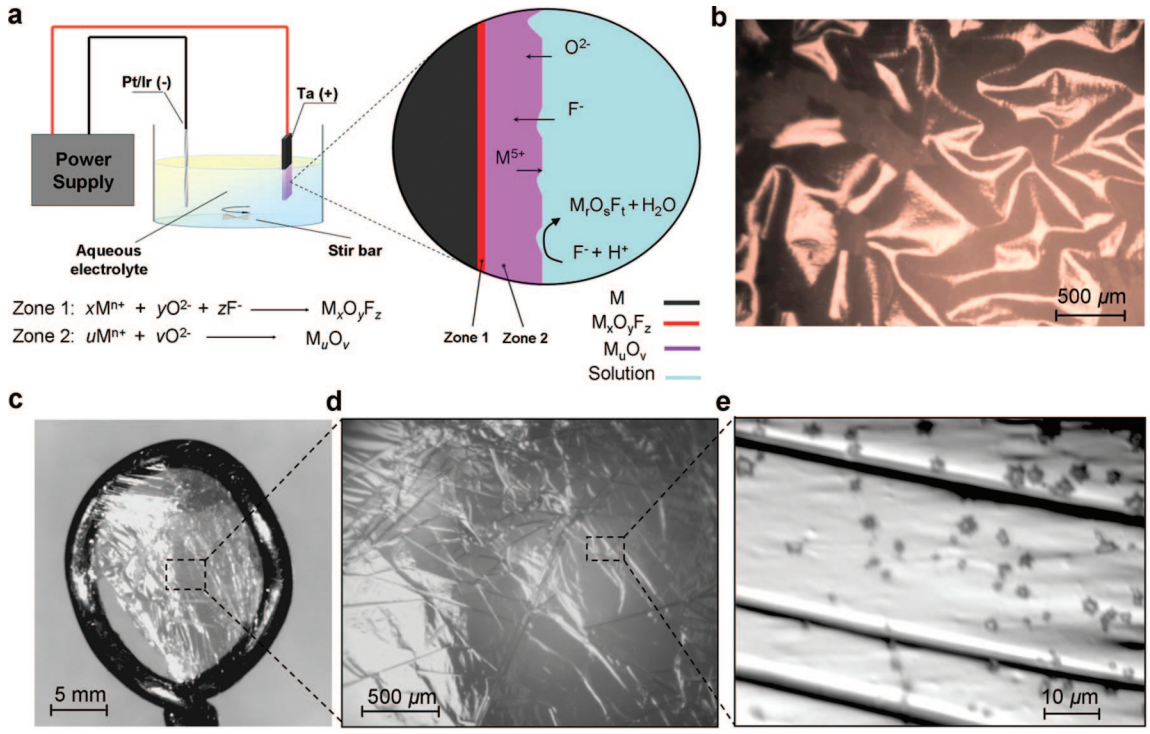

Figure 1. Preparation of transition metal oxide films by anodization. (a) Schematic diagram showing the anodic growth of the oxide film. (b) Optical image showing a detached 80 nm thick Nb_2O_5 membrane on filter paper. (c–e) Optical images of a 40 nm thick free-standing Ta_2O_5 membrane supported by a wire loop in air. The membrane is highly reflective in nature.

a sacrificial layer for the detachment of the metal oxide membranes from the underlying base metal surface.

In extension of the differential migration concept to other transition metal oxides, we now report a generic method for the fabrication of detachable, porous, and uniform ultrathin films of Nb_2O_5, TiO_2, Ta_2O_5, or WO_3 with controllable thickness (from 30 to 150 nm). In order to generalize the method on other metals, we had to further elucidate the details behind the mechanism enabling the tantalum oxide films to separate from the bulk metal surface. Good control over the size and degree of porosity of these free-standing membranes was achieved by varying reaction parameters such as etchant solution concentration, voltage, and reaction time. In addition to having shown catalytic activity, Nb_2O_5, TiO_2, Ta_2O_5, and WO_3 have desirable properties such as high melting points, high refractive indices, piezoelectricity, hardness, high dielectric constants, and excellent chemical stability, which make these films relevant to applications in catalysis, optics, waveguides, electronics, supercapacitors, sensing, *etc.*[30−32]

RESULTS AND DISCUSSION

Fabrication of Nanomembranes. The fabrication process encompasses three steps: electropolishing, oxide growth, and oxide sheet separation. Four different types of oxide sheets (Nb_2O_5, TiO_2, WO_3, and Ta_2O_5) were formed. Nb_2O_5, TiO_2, WO_3, and Ta_2O_5 films were grown on electropolished Nb, Ti, W, and Ta substrate surfaces by anodic oxidation in aqueous electrolytes containing either NH_4F or a mixture of HF and H_2SO_4 using a conventional two-electrode system (Figure 1a). The anodization conditions used for each specific metal are mentioned near its discussion.

Growth of Metal Oxide Films. Metal oxide films are formed during anodic oxidation due to the migration of ionic species (F^-, O^{2-}, OH^-) from the electrolyte toward the metal/metal−oxide interface and M^{n+} from the metal toward the oxide electrolyte interface under the applied potential (Figure 1a, inset). A thin layer rich in metal oxyfluoride forms *in situ* at the metal/metal−oxide interface during anodization due to the higher mobility of F^- compared to O^{2-} in a sufficiently high electric field gradient as shown in zone 1 of Figure 1a. This oxyfluoride layer provides the sacrificial layer for the detachment of the metal oxide membranes from the underlying base metal surface. In contrast to cases in which the thin film is grown on top of the sacrifical layer,[20−22] in our case, the sacrificial layer grows *in situ* during the formation of oxide in the same electrolyte solution, making the process simpler and straightforward. In addition to being responsible for the detachment, the fluoride ions also etch the oxide under acidic conditions to make it porous. Figure 1b−e shows typical optical images of the detached Nb_2O_5 and Ta_2O_5 membranes on filter paper and wire loop. It should be noted that the lines in the zoomed-in images of the Ta_2O_5 membrane (Figure 1d,e) represent folds (with no cracks) developed during the transfer of the membrane from the air/water interface to the wire loop, demonstrating the excellent mechanical properties of these membranes.[33,34]

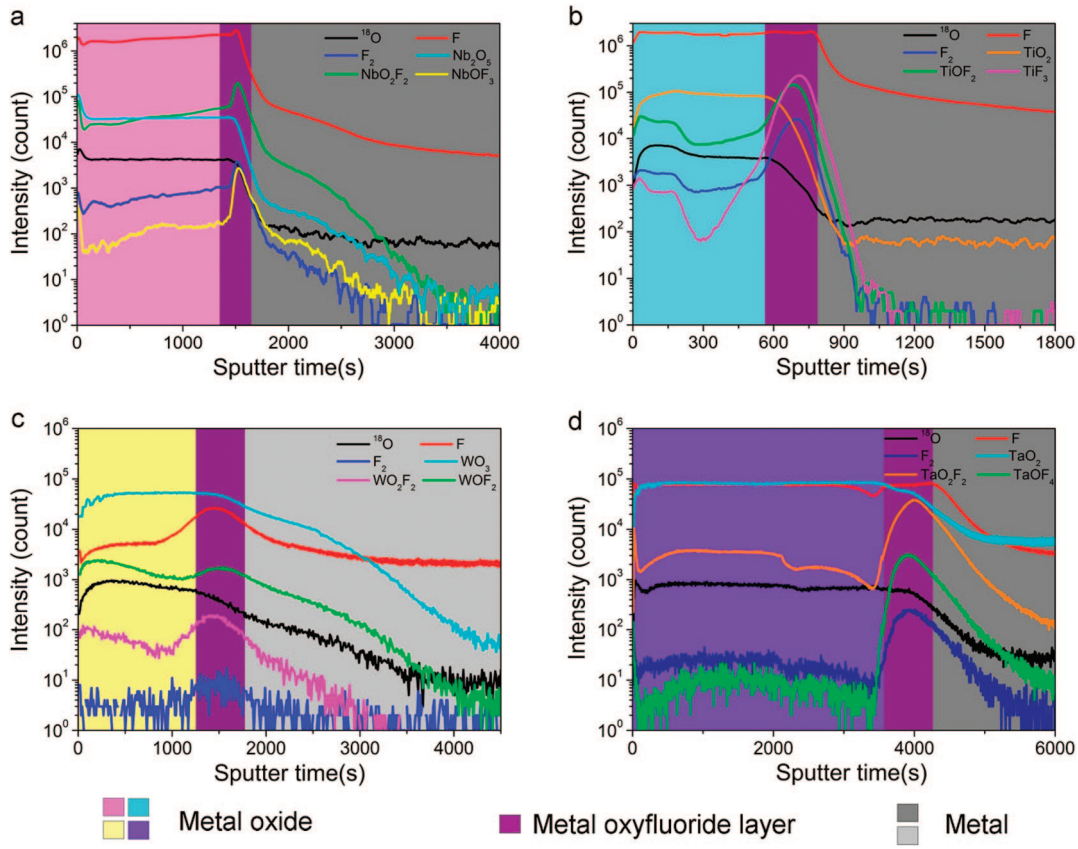

Figure 2. ToF-SIMS depth profiling data of detachable Ta_2O_5, Nb_2O_5, WO_3, and TiO_2. All of the depth profiles show a pronounced spike in the fluoride concentration at the metal/metal−oxide interface as shown by the dark areas. (a) Depth profile of Nb_2O_5 film grown for 10 s at 100 V. (b) Depth profile of a TiO_2 film grown for 20 s at 60 V. (c) Depth profile of a WO_3 film grown for 1 min at 50 V. (d) Depth profile of a Ta_2O_5 film grown for 1 min at 50 V.

We performed depth profiling time-of-flight secondary ion mass spectrometry (TOF-SIMS) on the Nb_2O_5, TiO_2, WO_3, and Ta_2O_5 films to observe the changes in film chemistry as a function of depth under their specific fabrication conditions. The ToF-SIMS depth profiles of Nb_2O_5 (Figure 2a; 1 M NH_4F, 100 V, 10 s), TiO_2 (Figure 2b; 1 M NH_4F, 60 V, 10 s), WO_3 (Figure 2c: 1 M NH_4F, 50 V, 1 min), and Ta_2O_5 (Figure 2d; 1 M NH_4F, 20 V, 1 min) reveal the oxide/oxyfluoride/metal multilayer structure of the system. A very pronounced spike in the fluoride concentration at the metal/metal−oxide interface confirms the presence of a thin layer (approximately 5 nm) consisting of a broad range of different metal−oxyfluoride compounds such as TaF_5, TaO_2F, $TaOF_3$, *etc.* (in the case of tantalum); Nb_2O_5, NbO_2F, $NbOF_3$, *etc.* (in the case of niobium); $TiOF_2$ and TiF_4 (in the case of titanium), and WO_2F_2 and WOF_4 (in the case of tungsten). This thin layer forms because various anions (F^-, O^{2-}, OH^-) and metal cations M^{n+} combine in many different ways at the interface to give rise to this oxyfluoride compound mixture. Many different ions observed in SIMS can also occur as the result of recombination (after the sputter event). This layer forms preferentially at the interface and not inside the metal oxide because of the fast migration of F^- ions as compared to O^{2-} and OH^- under the high applied electric field (material specific but generally from 20 to 50 V). It is this very thin layer which results in poor adhesion of the metal oxide films to the underlying substrate.

Control Over Thickness of Membranes. The thickness of each metal oxide membrane sample can be controlled by adjusting the applied voltage and time of anodization and is in the range of 30−150 nm under the current preparative conditions. However, the thickness of the oxide films has a substantial effect on their adhesion to the underlying metal surface. The detachment becomes progressively difficult with an increase in film thickness, requiring a larger peeling force. In general, films thinner than 150 nm are easiest to detach. The considerable increase in adhesion for thicker oxide films results from the decrease in fluoride ion migration speed due to a decrease in the magnitude of the field gradient within the film as the thickness of oxide membranes increases (see ref 23 and Supporting Information). Detachment of thicker oxide films is possible under higher applied voltages, but care must be taken to avoid sample burn because of dielectric breakdown. This can be circumvented if the applied potential is increased gradually.

Detachment of Oxide Films. Detachment behavior also varies between different metal oxide membranes. The tantalum and niobium oxide sheets were separated

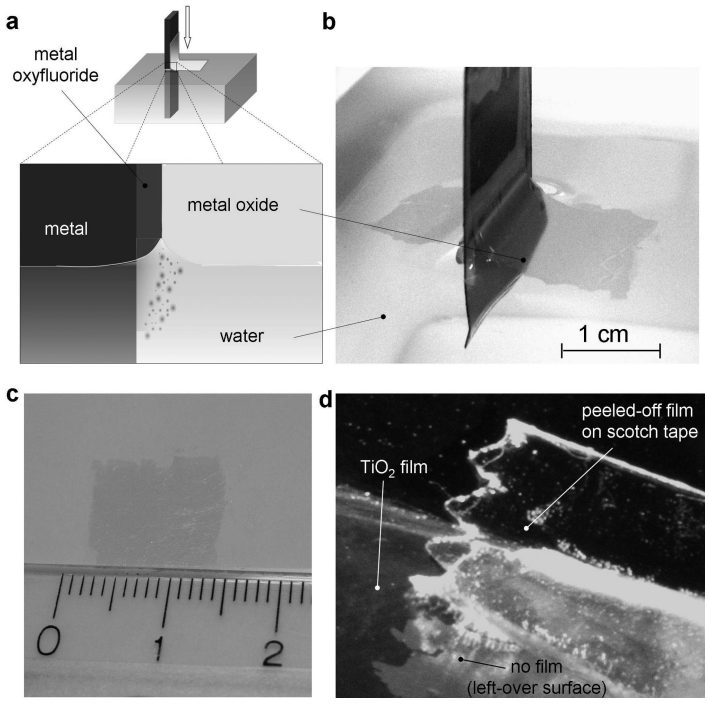

Figure 3. Illustration showing the film peeling process. (a) The architecture of the oxide film composition shown as separated layers. The film detaches due to the dissolution of the fluoride-rich layer in water and floats off due to the skin effect. (b) Micrograph of a partially detached and floating tantalum oxide film over water surface. (c) Micrograph of a Ta_2O_5 nanofilm detached from the substrate and transferred on to glass slide. (d) Scotch tape peeling off a TiO_2 film (<100 nm).

from the bulk metal using the lift-off−float-on (LOFO) technique or ultrasonication with deionized water.[23] The LOFO technique only succeeds for thin tantalum and niobium oxide films but not for tungsten and titanium oxide films. Figure 3a,b shows the LOFO process in which water enters into the interfacial region of the freshly grown oxide on its metal substrate and dissolves the metal fluoride salts, thereby inducing separation. Tantalum oxide membranes are easier to detach as one big sheet (up to 2×3 cm^2 were fabricated, limited by the size of our equipment), while niobium oxide membranes break up into small shards of a few square millimeters in size during separation due to different mechanical properties. However, the mechanical properties may be enhanced by using alloys of the particular metals.

The inorganic TiO_2 and WO_3 films were difficult to detach using the LOFO technique but can be easily peeled-off using scotch tape (Figure 3d). This can be attributed to the difference in the solubility of the oxyfluoride layers for these four kinds of samples. Tantalum and niobium oxyfluoride species are fairly soluble in water, while their tungsten and titanium counterparts are unstable and insoluble.[35,36] A possible solution for fabricating self-supporting membranes of titanium and tungsten oxide is to detach the oxide films with an adhesive polymer followed by a rinse with solvent to regain a pure metal oxide. Alternatively, the transfer printing technique developed by Rogers and co-workers can be applied to these films.[37,38]

In order to further investigate the mechanism of fluoride ion migration and detachment, ToF-SIMS and X-ray photoelectron spectroscopy (XPS) measurements were performed on sequentially prepared different tantalum oxide samples. Similar effects were found in case of Ti, Nb, and W oxide membranes, indicating the generality of the observed phenomenon.

XPS analysis of the backside of peeled-off Ta_2O_5 membranes and left-over surfaces before and after rinsing them with water yielded important information on the presence and constitution of the oxyfluoride layer. The XPS spectra of the underlying tantalum surface after peeling of a 40 nm thick film formed by anodizing an electropol-

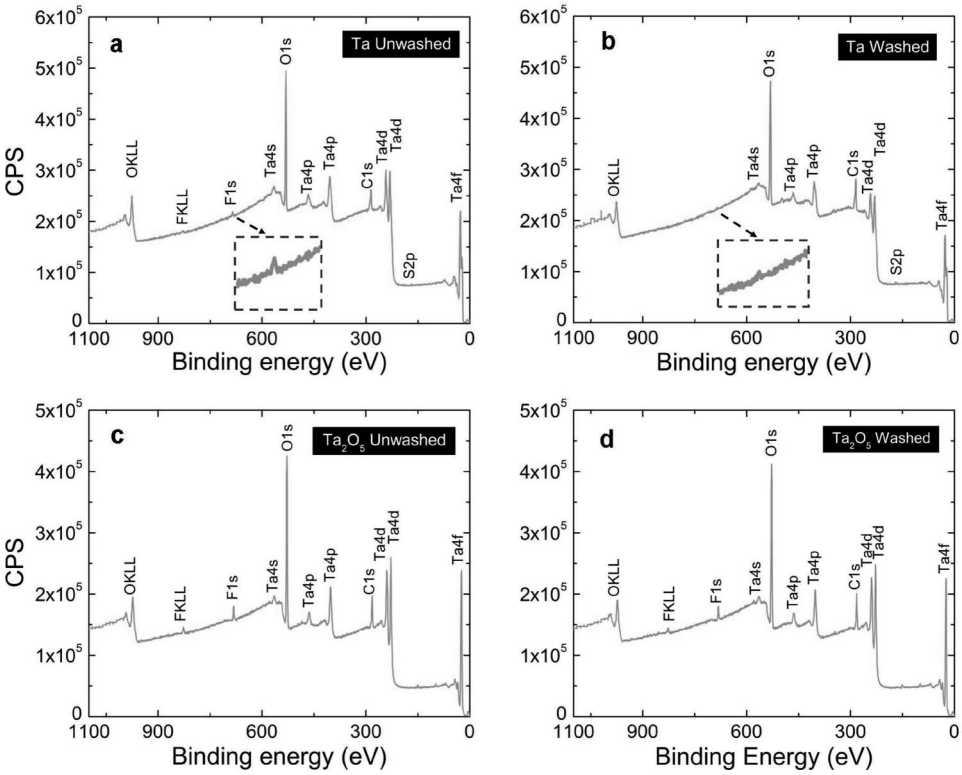

Figure 4. Survey XPS spectra of the left-over tantalum surface after peeling a tantalum oxide membrane grown for 1 min at 20 V in 1 M NH_4F solution (a) before washing with water (b) after washing. Inset magnification is 5×. Survey XPS spectra of the backside of the peeled off oxide membrane (c) before washing with water (d) after washing. The data show that the fluorine peak disappears after washing the tantalum metal but does not change after washing the oxide membrane.

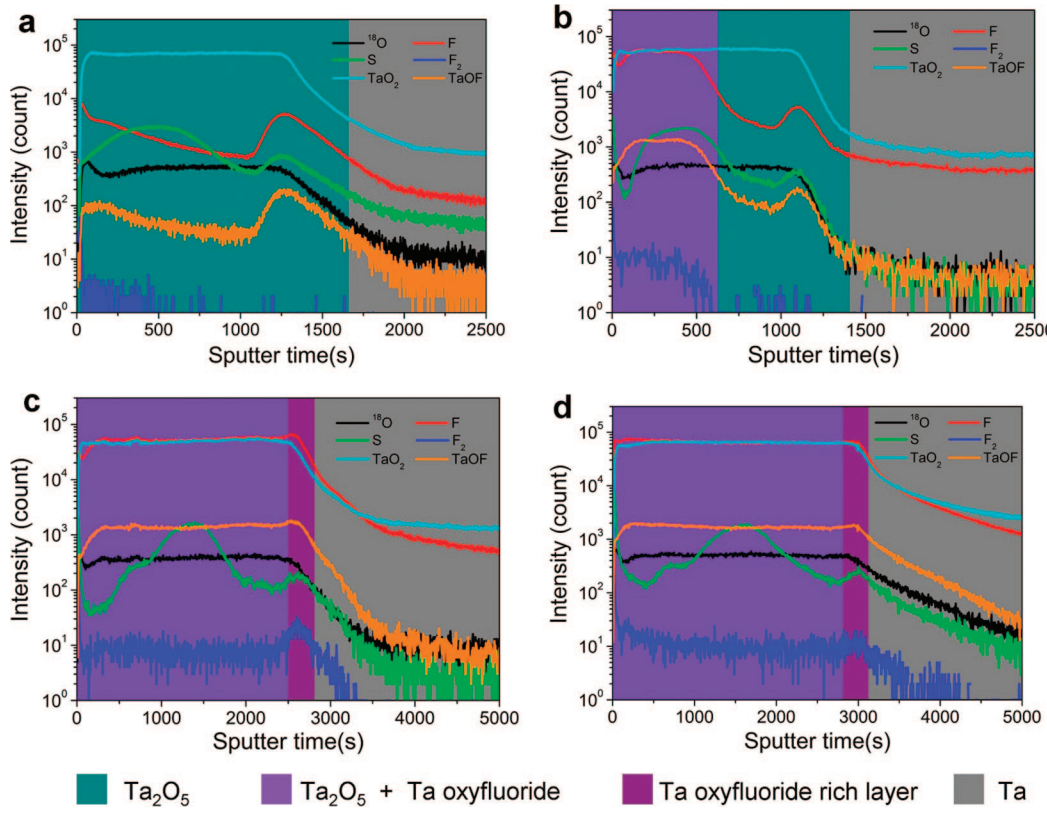

Figure 5. ToF-SIMS depth profiles of Ta_2O_5 films on a tantalum substrate, demonstrating the differential migration of fluoride ions under specific electric field strengths after sample-specific anodization treatments. (a) Sample #1: Inseparable Ta_2O_5 film grown for 1 min at 20 V in 1 M H_2SO_4 electrolyte (<0.1 wt % HF added). (b) Sample #2: Inseparable film grown for 1 min at 20 V in 1 M H_2SO_4 and then for 1 min at 30 V in 1 M NH_4F electrolyte. (c) Sample #3: Separable film grown for 1 min under 20 V in 1 M H_2SO_4 and then for 1 min at 60 V in 1 M NH_4F electrolyte. (d) Sample #4: Separable film grown for 1 min at 20 V in 1 M H_2SO_4 and then for 5 s at 60 V in 1 M NH_4F electrolyte.

ished tantalum foil for 1 min in 1 M NH_4F solution at 20 V show a thin layer of fluoride species on the surface (Figure 4a). This oxyfluoride layer can be removed by rinsing the substrate in Millipore water for 5 s, confirming that this tantalum oxyfluoride layer is highly soluble in water (Figure 4b). On the other hand, there is no significant difference in the XPS survey spectra of the backside of the detached Ta_2O_5 membrane before and after washing (Figure 4c,d). This means that the oxyfluoride layer is adherent to the base metal surface rather than the tantalum oxide membrane, making them free of the oxyfluoride species. However, there is slight incorporation of fluorine into the membranes. This is expected because tantalum oxide films grown by anodization are known to incorporate electrolyte anions (F^-) throughout the entire film.[39]

We also examined the composition of the above-mentioned tantalum oxide membranes using depth profiling ToF-SIMS after detaching and transferring them onto a silicon surface using the LOFO technique. The SIMS profile (Supporting Information) shows that there is no sharp fluoride peak at the silicon/Ta_2O_5 interface, confirming that the oxyfluoride layer dissolves in water.

Differential Migration of Fluoride Anions. A series of experiments were performed in conjunction with ToF-SIMS depth profiling to determine the effect of concentration, voltage, and time on the migration of electrolyte ions, specifically, F^- ions. Samples of tantalum metal were prepared by anodizing electropolished foils at 20 V for 1 min in 1 M H_2SO_4 electrolyte solution containing trace amounts of fluoride (<0.01 wt % HF). A second anodization step in 1 M NH_4F solution followed the first step for samples #2−#4 at sample-specific voltages and anodization times. ToF-SIMS depth profiles were then obtained. The peak in the resulting depth profile of sample #1 (Figure 5a) indicates the presence of fluoride at the metal/metal−oxide interface. However, the oxide could not be separated, implying that the amount of fluoride at the interface was insufficient to allow for detachment. Comparing Figures 5a−d and 2d, the relevant criterion in the case of tantalum is that the ratio of the F signal to the TaO_2 signal in the ToF-SIMS profiles should be at least 1 for detachment. In the case of other oxides, a similar benchmark could presumably be established. The oxide layer of sample #2, prepared by re-anodizing sample #1 at 30 V in 1 M NH_4F solution for 1 min, was also inseparable because the applied potential difference was not large enough to migrate the F^-

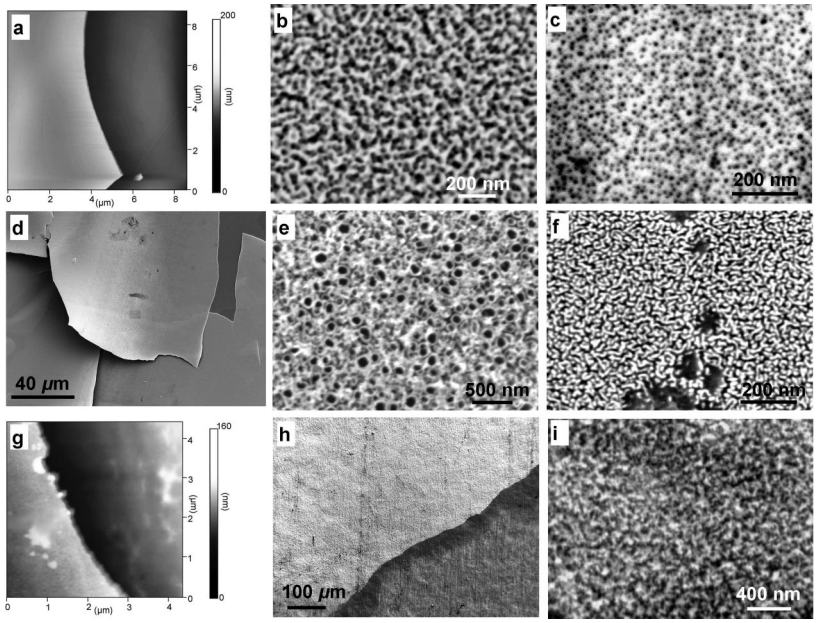

Figure 6. Scanning electron microscope (SEM) and atomic force microscope (AFM) micrographs of Nb_2O_5, TiO_2, and WO_3 membranes with modulated surface morphology and porosity. (a) AFM image of the edge of an 80 nm thick Nb_2O_5 sheet grown for 5 min in 0.5 wt % HF at 20 V, showing an rms surface roughness of 2.6 nm. (b) SEM image of a Nb_2O_5 film with dimples but no visible pores grown for 5 min in 1 wt % HF at 20 V. (c) Nb_2O_5 film grown for 20 s at 100 V in 0.5 M NH_4F + 1 M H_2SO_4 electrolyte. (d,e) SEM images of a TiO_2 film with small ordered pores grown for 5 min in 2 wt % HF at 20 V, (f) and with disordered random porous morphology grown in 1 M NH_4F for 20 s at 60 V. (g) AFM image of the edge of a 60 nm thick WO_3 sheet grown for 1 min in 0.5 M NH_4F at 50 V, showing an rms surface roughness of 7.2 nm. (h,i) SEM images of the same WO_3 film as shown in (g).

ions to the interface. The ToF-SIMS depth profile (Figure 5b) shows that the fluoride from the first experiment remains in the sample. A Ta_2O_5 layer (green shading) remains between the freshly migrated Ta oxyfluoride region and the metal/metal−oxide (located at $x \sim 1400$ s, Figure 5b) interface. An oxide that is too thick will not let the fluoride ions pass at low voltages.

Given a sufficiently high potential gradient across the oxide film, fluoride ions will migrate rapidly into and across the film. Sample #3 was prepared by, after the initial step, anodization for 1 min at 60 V in 1 M NH_4F electrolyte, that is, at a higher potential. The ToF-SIMS depth profile (Figure 5c) shows a uniformly distributed region of fluorine from the oxide film surface to the metal/metal−oxide interface. In this case, the obtained film was detachable from the surface, indicating that a sufficient amount of fluoride had migrated to the interface. This shows that there is sufficient F^- in solution and that the driving force (electric field) was sufficient to migrate a sufficient amount of F^- to the interfacial region. Recent work of Shimizu and co-workers has shown that the fluoride anions migrate toward the metal substrate at a rate which is 1.85 times faster than that of oxygen ions under an appropriate voltage (approximately 80 V).[29] Sample #4 (Figure 5d) was prepared by re-anodizing sample #1 at 60 V in 1 M NH_4F for 5 s instead of the usual 1 min in the second anodization step. The difference in resulting film thickness reflects itself in the difference in sputter time required to reach the interface, although we did not attempt a precise calibration with respect to absolute film thickness. This film was also separable, implying that fluoride ions migrate toward the interface not by etching the oxide (as the anodization time is negligible) but by physically passing through the amorphous oxide.

Nonporous membranes were also made by growing the oxide in an electrolyte solution which does not contain fluoride species, such as 1 M H_2SO_4. The films were then put in 1 M NaF solution, and a potential of 60 V was applied. The films were detached if they were less than 100 nm thick. This shows that F^- migrates to the interface by passing through the amorphous oxide layer. However, the resulting films do not show any sign of porosity which is due to the lack of sufficient etching by F^- ions in the absence of adequate H^+ ions. These experiments show that fluoride concentration and applied potential should be above a minimum threshold value for the separation of metal oxide membranes from the base metal surface. However, the values can differ from metal to metal.

Porosity. The presence of fluoride ions in the electrolyte solution dictates the degree of separability and porosity of the oxide films during their fabrication. The small amount of fluoride is not only responsible for the film detachment but also causes a particularly rapid dissolution of the formed oxide, thereby making the resultant oxide sheet porous.

$$M_xO_y + zF^- + yH^+ \rightarrow MF_z^- + yH_2O \quad (1)$$

The porous surface morphology of the metal oxide films is confirmed by analyzing their surface morphology using scanning electron microscope (SEM) and atomic force microscope (AFM) imaging. The images in Figure 6 and Figure 7 show the porous nature of the fabricated Nb_2O_5, TiO_2, WO_3, and Ta_2O_5 films. The quality and degree of porosity depends greatly upon the type and concentration of the electrolyte solution used during anodization. Porous Nb_2O_5 oxide sheets (Figure 6a−c) have disordered rough pores (Figure 6b) when anodized in 1 wt % HF and have circular and evenly distributed pores (Figure 6c) when a 0.5 M NH_4F + 1 M H_2SO_4 electrolyte solution is used for anodization. TiO_2 films (Figure 6d−f) have either a tubular structure or a random surface morphology. The formation of tubular nanostructures is more favorable in solutions with a lower pH.[40,41] The surface morphology of WO_3 films is very rough and has highly disordered pores (Figure

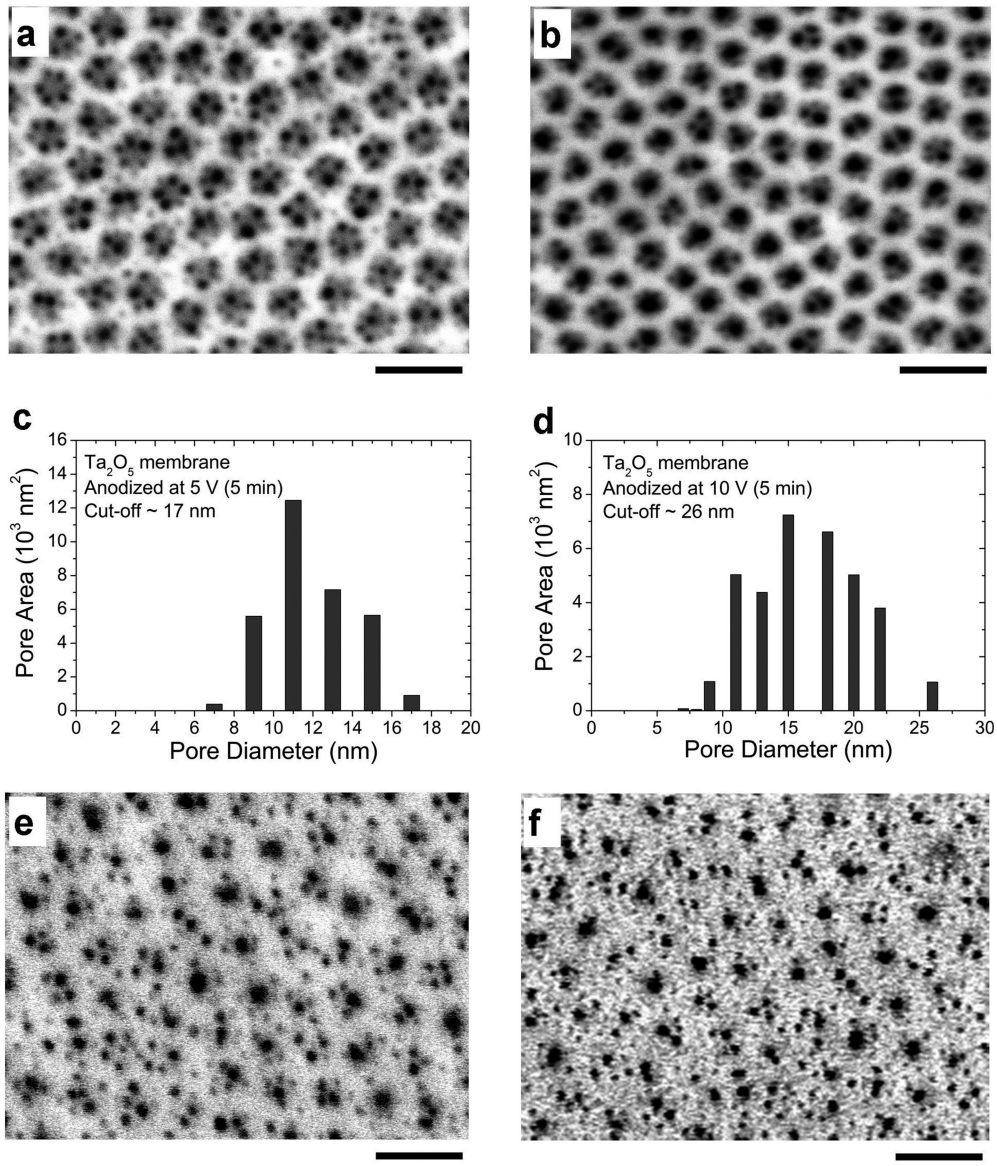

Figure 7. Effect of voltage on the pore size distribution in Ta_2O_5 membranes. Anodic anodization was carried out on mirror-finished tantalum substrates having highly ordered dimpled morphology.[43] SEM micrographs of an oxide film with small pores aligned with dimples grown for 5 min in 1 M H_2SO_4 and 2 wt % HF at constant voltage of (a) 5 V and (b) 10 V. (c,d) Histograms generated from (a) and (b) showing the maximum (cutoff) pore size and porosity increase by changing the applied potential from 5 to 10 V. (e) SEM image of an oxide film with small pores grown for 5 min in 1 M H_2SO_4 and 2 wt % HF at constant voltage of 15 V and (f) 20 V, showing the etching at the top of the ridges and the deterioration of the alignment of the pores with dimples. Scale bars correspond to 100 nm.

6g−i). The energy-dispersive X-ray microanalysis spectra (see Supporting Information) of peeled-off Nb_2O_5, TiO_2, WO_3, and Ta_2O_5 membranes on carbon tape show that these membranes are purely inorganic in nature with no other impurities detected. Recently, similar nanostructured silicon oxide surfaces with disordered pores (~10 nm in size) prepared by anodic oxidation/etching have found an application in nanostructure−initiator mass spectrometry (NIMS), where the nanostructure of the surface helps in trapping desired molecules.[42]

Modulating Pore Size with Voltage. We will now discuss control of the pore size and number primarily in tantalum oxide membranes. The electropolishing step generates highly ordered nanodimples on the metal surface as outlined in a previous paper.[43] The dimpled morphology of the starting electropolished tantalum surface provides a handle in adjusting the number of pores inside each dimple of the dimpled Ta_2O_5 membranes. Previously, we showed control over the pore size by changing the concentration of the solution. Here we now show that the applied voltage provides a better handle in controlling the number and size of pores inside a dimple. The potential was kept constant during anodization, and the current generally starts around 4 mA/cm^2 and gradually decreases as the oxide film

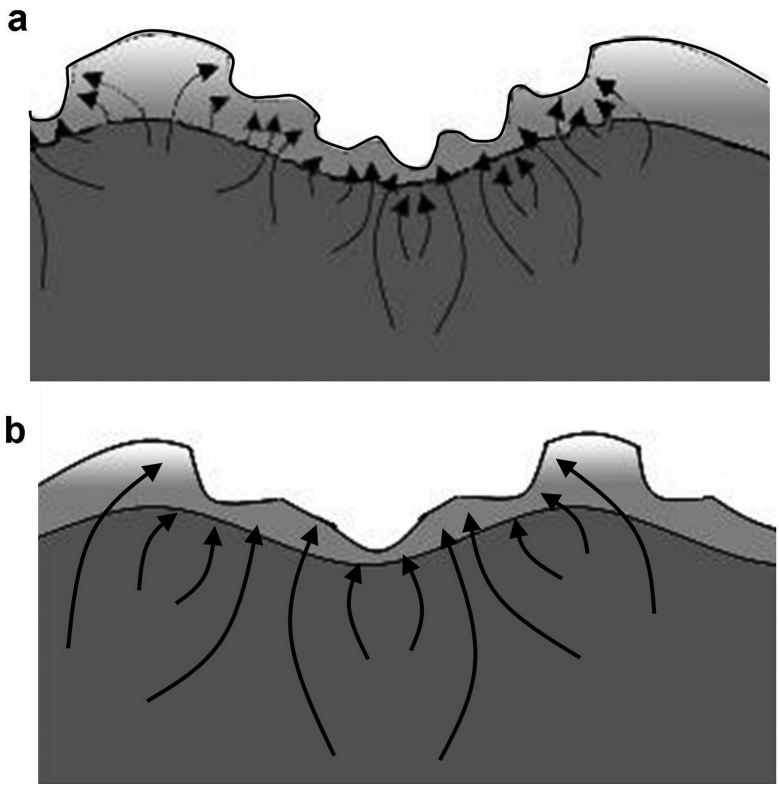

Figure 8. Schematic diagram showing the tunability of size and number of pores caused by variance of the strength of the applied electric field inside each dimple in Ta_2O_5 membranes. (a) Low electric field. (b) High electric field.

grows with time. Well-controlled pores inside membranes are only observed under specific conditions as discussed below.

Smaller and more numerous pores are formed inside the dimple morphology of the membranes (Figure 7a and Supporting Information) at lower voltages (5 V) by anodizing the dimpled tantalum surface in 1 M H_2SO_4, 2 wt % HF for 5 min. As the voltage is increased to 10 V, the number of pores inside each dimple decreases, but their size increases (Figure 7b and Supporting Information). If the pores in these two images are binned according to their size in 2 nm steps and the total area corresponding to each pore size is plotted (Figure 7c,d), an increase in dominant pore diameter with voltage is seen. Higher voltages, however, also lead to a somewhat larger spread in pore diameters. This ordering of pores is possible only at low voltages (~10 V) as films start to burn at higher voltages (more than 25 V) due to dielectric breakdown under the corrosive acid attack. Also, the pores start to form on the ridges of the dimples, and the order deteriorates at voltages from 12 to 25 V (Figure 7e,f).

The tunability of the number and size of the pores can be explained as localized etching that depends on the strength of the applied electric field. Low electric fields cause a localized electrolysis of water (generating H^+) and therefore a local etching (eq 2) of tantalum oxide that results in smaller pores (Figures 7b and 8b) due to the dissolution of the final products. High electric fields cause the electrolysis of water and the etching of the metal oxide to occur on a larger surface area that leads to the creation of bigger pores (Figures 7b and 8b).

$$Ta_2O_5 + 14F^- + 10H^+ \rightarrow 2TaF_7^- + 5H_2O \quad (2)$$

The electric field is more intense at the sections of the dimple, with greater curvature causing the etching reaction to take place exclusively inside the dimple. As the electric field is increased from 10 V to 15 or 20 V, the etching also becomes more intense at the crest of the dimple. The pores starts to appear everywhere, but still the pores inside the dimples (Figure 7e,f) are larger in diameter than those on the ridges due to the higher electric field inside the dimples as compared to that on the ridges. The ability to control and guide the size and number of pores in Ta_2O_5 membranes may be useful for nanosieve filtration applications or for catalysts or catalyst supports with ultrashort contact times. Additionally, the numerous pores inside these membranes increase the surface area and could allow further chemical functionalization to further enhance their physical and chemical properties.

Not all pores penetrate the dimpled membrane, as is evident from TEM micrographs taken of Ta_2O_5 membranes (Figure 9). However, more pores can be generated and their size further tuned by either annealing the tantalum oxide membranes to around 700 °C or chemically etching them under appropriate conditions to remove the barrier layer.[3,44,45] Annealing results in a volume change (preferably contraction) of the material due to phase transformation and crystallization, whereas etching will remove the material.

CONCLUSION

In summary, a simple and versatile method has been developed for fabricating purely inorganic, high-quality ultrathin membranes of transition metal oxides with nanoscale thickness (<100 nm). The thinnest square centimeter sized films we have produced and separated are around 30 nm thick, but this does not represent the lower limit. The thickness range of the films is determined by their mechanical properties and the desired area, with tantalum oxide being the most robust material tested by us. The membranes are riddled with small pores, and anodization allows for fine-tuning of the pore size in the oxide membranes *via* manipulation of the applied potential during growth. We have therefore generalized the concept of differential migration of fluoride ions under the applied potential. Fluorine chemistry is traditionally associated with safety concerns, but the discovery of more stable and effectively more controllable fluorinating agents

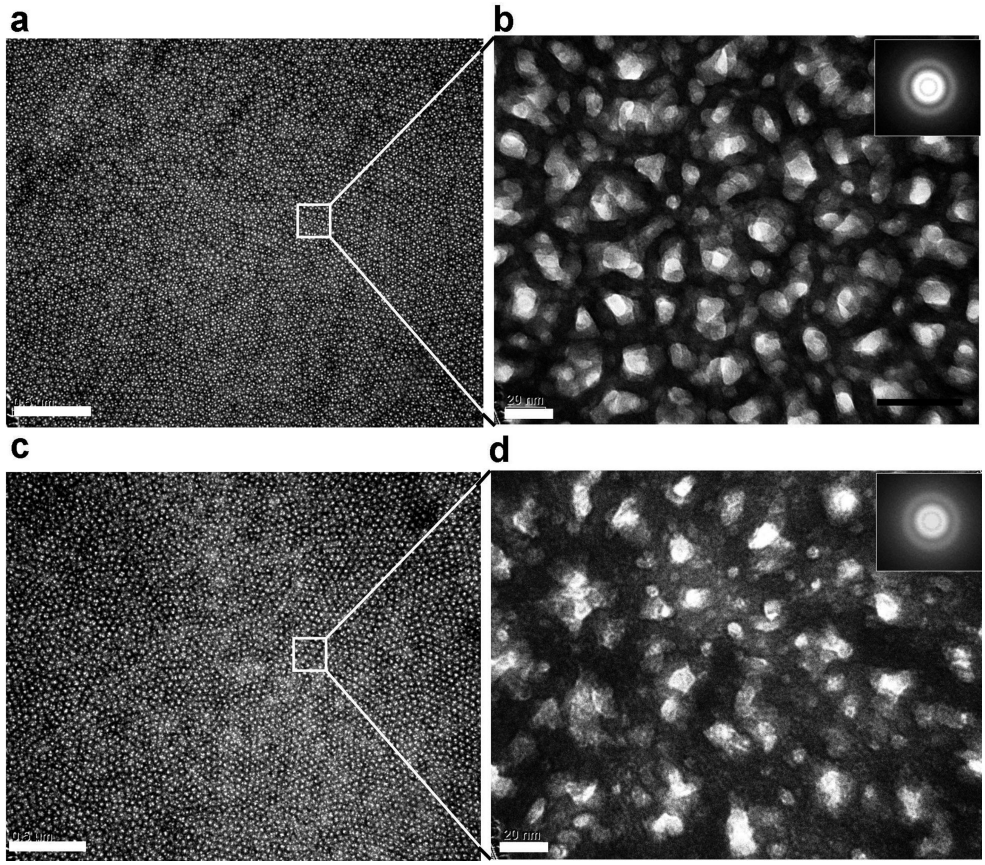

Figure 9. TEM micrographs of Ta_2O_5 membranes with pores grown for 5 min in 2 wt % HF under (a,b) a low electric field (5 V) and (c,d) a high electric field (10 V). Pores near the center of the dimples penetrate deeper than pores at the ridges. Scale bars correspond to 500 nm for (a,c) and to 20 nm for (b,d). Diffuse electron diffraction pattern (insets of b and d) indicates that the oxide in the membranes is amorphous.

has opened up a variety of possibilities in the pharmaceutical and silicon industry due to its usefulness in etching and lead optimization made possible by its binding efficacy, selectivity, and unique molecular properties.[46] The unique properties of fluorine are also the key to the process demonstrated here because it weakens the adhesion of the metal substrate to its protective oxide layer by migrating from the electrolyte solution to the metal/metal−oxide interface under an applied potential difference. This understanding of the fast fluoride ion migration under applied electric fields may be relevant in other technical developments, for example, elucidating the role of the LiF layer in organic light-emitting diodes (OLEDs).[47] Our membranes will find use as self-supporting materials in the fields of catalysis, filtration, optics, sensors, and dielectric spacers. The tunable porosity of very thin membranes, in particular, makes them suitable for the filtration of biomolecules and nanoparticles,[3] in which case antifouling properties and mechanical strength become very important. Reactant flow through thin catalytic membranes is also of importance in heterogeneous catalytic processes where selectivity is achieved though ultrashort contact times.[48] While it is possible to load membranes with catalyst particles, many transition metal oxides have catalytic properties themselves. Since the process presented here is not limited to a particular oxide, the fabrication of porous membranes directly out of a catalytically active oxide becomes feasible.

METHODS

Materials. H_2SO_4 (95−98%, reagent grade) and HF (48%) were purchased from Fisher Scientific, and NH_4F (40%, semiconductor grade) was purchased from Sigma-Aldrich. Acetone, methanol, and ethanol (all semiconductor grade) were bought from Fisher Scientific. All chemicals were used as received without any further modification.

Electrochemical Setup for Electropolishing and Oxide Growth. The electrochemical cell was a two-electrode system consisting of a Pt/Ir (0.25 mm diameter) wire acting as the counter electrode and the cleaned metal foils as the working electrode (anode) connected to a power supply (Agilent E3615A). The distance between the working and counter electrodes was kept at approximately 1.5 cm. During electropolishing and anodization, the solution was stirred using a magnetic stir bar. Freshly mixed electrolytic solutions typically need to settle for 16−20 h before the first sample is processed. All experiments were performed at room temperature (approximately 20 °C).

Fabrication of Membranes. The titanium (Ti) foil (Alfa-Aesar, 99.99%, 0.127 mm), tungsten (W) ribbon (Alfa-Aesar, 99.95%,

0.125 mm), tantalum (Ta) foil (Alfa-Aesar, 99.95%, 0.127 mm), and niobium (Nb) foil (Alfa-Aesar, 99.97%, 0.127 mm) samples used in this study were mechanically cut and rinsed with acetone, methanol, and then with Millipore water (18.2 MΩ · cm resistivity) and then dried under argon flow before anodizing them. This was followed by electropolishing with a voltage of 15 V in a (v/v 9:1 for Nb and Ta, v/v 8:2 for Ti, and v/v 93:7 for W) mixture of concentrated H_2SO_4 (95−98% reagent grade) and HF (48%) for 5 min for Nb and Ta, 1 min for Ti, and 10 min for W. Freshly electropolished Nb, Ti, W, and Ta foils were rinsed thoroughly in Millipore water and then were ultrasonicated in water to remove any fluoride contamination and were finally dried under argon flow. These electropolished metal samples were subjected to anodization for specific times at constant voltages between 20 to 100 V in either NH_4F solution or a mixture of HF and H_2SO_4 to grow metal oxide films. The metal films can be detached from the base metal by the LOFO technique for Ta_2O_5 and Nb_2O_5 films or by scotch tape for TiO_2, WO_3, Ta_2O_5, and Nb_2O_5 films.

Characterization. SEM imaging was performed with a JEOL JSM-7000F scanning electron microscope, equipped with a Schottky-type field emission gun (FEG) filament. Energy-dispersive X-ray (EDX) spectroscopy was carried out using a 10 kV accelerating voltage. INCA 300, EDX System (Oxford, UK) software was used for the data acquisition and analysis.

Atomic force microscopy was performed in tapping mode on a Veeco Enviroscope with a Nanoscope IIIa controller and Veeco RTESP p-doped Si tips with a nominal radius of less than 10 nm. The thickness of the metal oxide membranes was assessed by measuring the step height at the peeled-off edges using AFM.

XPS spectra were recorded on a Kratos Axis ultra X-ray photoelectron spectrometer with a base pressure of 1×10^{-10} mbar employing monochromatic Al Kα X-ray source (1486.71 eV) and charge neutralizer system. XPS survey scans were taken at a pass energy of 160 eV with step sizes of 0.7 eV in an area 300 μm × 700 μm in size.

Quantitative SIMS analysis was carried out on a ToF-SIMS IV instrument (ION-TOF GmbH) equipped with a bismuth liquid metal ion source (LMIG). The primary analysis beam was pulsed 25 keV, Bi^+ with a ∼1.5 μm spot size and a target current of ∼0.6 pA. The Bi^+ primary beam was rastered over a 100 μm × 100 μm area. Secondary ions were extracted, and mass was separated *via* a single reflectron-type ToF analyzer. The mass resolution for this work was ∼10 000 above 200 amu, and the mass range was 0−1000 amu. Due to the insulating nature of the samples, a pulsed electron flood gun was employed for charge neutralization. For depth profiling, a second 3 keV Cs^+ beam was used to sputter a 250 μm × 250 μm area, with the Bi^+ analysis area centered within region to avoid edge effects. Since the species of interest included mainly F, S, and O as well as oxides and possible oxyfluorides of metals, negative secondary ions were monitored.

High-resolution TEM was carried out with a JEOL 2010 field emission TEM/STEM, operating at an accelerating voltage of 200 kV.

Optical images were taken by a high-resolution microscope (Stereo Discovery.V12, maximum magnification 400×) equipped with a quartz−tungsten−halogen white light source.

Acknowledgment. We are grateful to Mark Biesinger (Surface Science Western) for providing the XPS analysis, Steve Koprich for help with SEM, Fred Pearson (both Brockhouse Institute for Materials Research) for help with TEM, and Kailash Kasala and Kalaichelvi Saravanamuttu for access to their optical microscope. The work was financially supported by the Natural Science and Engineering Research Council of Canada and an Ontario Premier's Research Excellence Award.

Supporting Information Available: Energy-dispersive X-ray microanalysis spectra of different transition metal oxide films and secondary ion mass spectrometry of thin tantalum oxide film on silicon as well as SEM micrographs of porous tantalum oxide membranes. This material is available free of charge *via* the Internet at http://pubs.acs.org.

REFERENCES AND NOTES

1. Baker, R. W. *Membrane Technology and Applications*; Wiley: Hoboken, NJ, 2004.
2. Xu, C.; Su, J.; Xu, X.; Liu, P.; Zhao, H.; Tian, F.; Ding, Y. Low Temperature CO Oxidation over Unsupported Nanoporous Gold. *J. Am. Chem. Soc.* **2007**, *129*, 42–43.
3. Striemer, C. C.; Gaborski, T. R.; McGrath, J. L.; Fauchet, P. M. Charge- and Size-Based Separation of Macromolecules Using Ultrathin Silicon Membranes. *Nature* **2007**, *445*, 749–753.
4. Kanellopoulos, N. K. *Recent Advances in Gas Separation by Microporous Ceramic Membranes*; Elsevier: Amsterdam, 2000.
5. Sakai, H.; Furukawa, Y.; Fujiwara, E.; Tada, H. Low-Voltage Organic Field-Effect Transistors with a Gate Insulator of Ta_2O_5 Formed by Sputtering. *Chem. Lett.* **2004**, *33*, 1172–1173.
6. Demiryont, H.; Sites, J. R.; Geib, K. Effects of Oxygen Content on the Optical Properties of Tantalum Oxide Films Deposited by Ion-Beam Sputtering. *Appl. Opt.* **1985**, *24*, 490–495.
7. Waldorf, A. J.; Dobrowolski, J. A.; Sullivan, B. T.; Plante, L. M. Optical Coatings Deposited by Reactive Ion Plating. *Appl. Opt.* **1993**, *32*, 5583–5593.
8. Sankur, H. O.; Gunning, W. J. Deposition of Optical Thin Films by Pulsed Laser Assisted Evaporation. *Appl. Opt.* **1989**, *28*, 2806–2808.
9. Gu, G.; Schmid, M.; Chiu, P. W.; Minett, A.; Fraysse, J.; Kim, G. T.; Roth, S.; Kozlov, M.; Munoz, E.; Baughman, R. H. V_2O_5 Nanofibre Sheet Actuators. *Nat. Mater.* **2003**, *2*, 316–319.
10. Yang, H.; Coombs, N.; Sokolov, I.; Ozin, G. A. Free-Standing and Oriented Mesoporous Silica Films Grown at the Air−Water Interface. *Nature* **1996**, *381*, 589–592.
11. Wang, X.; Lao, C.; Graugnard, E.; Summers, C. J.; Wang, Z. L. Large-Size Liftable Inverted-Nanobowl Sheets as Reusable Masks for Nanolithiography. *Nano Lett.* **2005**, *5*, 1784–1788.
12. Raman, N. K.; Brinker, C. J. Organic Template Approach to Molecular-Sieving Silica Membranes. *J. Membr. Sci.* **1995**, *105*, 273–279.
13. Jin, J.; Wakayama, Y.; Peng, X.; Ichinose, I. Surfactant-Assisted Fabrication of Free-Standing Inorganic Sheets Covering an Array of Micrometre-Sized Holes. *Nat. Mater.* **2007**, *6*, 686–691.
14. Baca, A. J.; Ahn, J.-H.; Sun, Y.; Meitl, M. A.; Menard, E.; Kim, H.-S.; Choi, W. M.; Kim, D.-H.; Huang, Y.; Rogers, J. A. Semiconductor Wires and Ribbons for High-Performance Flexible Electronics. *Angew. Chem., Int. Ed.* **2008**, *47*, 5524–5542.
15. Yuan, H.-C.; Kelly, M. M.; Savage, D. E.; Lagally, M. G.; Celler, G. K.; Ma, Z. Thermally Processed High-Mobility MOS Thin-Film Transistors on Transferable Single-Crystal Elastically Strain-Sharing Si/SiGe/Si Nanomembranes. *IEEE Trans. Electron Devices* **2008**, *55*, 810–815.
16. Arora, W. J.; Nichol, A. J.; Smith, H. I.; Barbastathis, G. Membrane Folding to Achieve Three-Dimensional Nanostructures: Nanopatterned Silicon Nitride Folded with Stressed Chromium Hinges. *Appl. Phys. Lett.* **2006**, *88*, 053108.
17. Malachias, A.; Mei, Y.; Annabattula, R. K.; Deneke, Ch.; Onck, P. R.; Schmidt, O. G. Wrinkled-up Nanochannel Networks: Long-Range Ordering, Scalability, and X-ray Investigation. *ACS Nano* **2008**, *2*, 1715–1721.
18. Mei, Y.; Kiravittaya, S.; Benyoucef, M.; Thurmer, D. J.; Zander, T.; Deneke, Ch.; Cavallo, F.; Rastelli, A.; Schmidt, O. G. Optical Properties of a Wrinkled Nanomembrane with Embedded Quantum Well. *Nano Lett.* **2007**, *7*, 1676–1679.
19. Schultz, M. J.; Zhang, X.; Unarunotai, S.; Khang, D.-Y.; Cao, Q.; Wang, C.; Lei, C.; MacLaren, S.; Soares, J. A. N. T.; Petrov,

I.; et al. Synthesis of Linked Carbon Monolayers: Films, Ballons, Tubes, and Pleated Sheets. *Proc. Natl. Acad. Sci. U.S.A.* **2008**, *105*, 7353–7358.
20. Lee, H.; Lee, S. W.; Goto, H.; Lee, S.; Lee, H.; Ha, J. S.; Goto, T.; Cho, M. W.; Yao, T.; Hong, S. Self-Separated Freestanding GaN Using a NH_4Cl Interlayer. *Appl. Phys. Lett.* **2007**, *91*, 192108.
21. Rogers, D. J.; Teherani, F. H.; Ougazzaden, A.; Gautier, S.; Divay, L.; Lusson, A.; Durand, O.; Wyczisk, F.; Garry, G.; Monteiro, T.; et al. Use of ZnO Thin Films as Sacrificial Templates for Metal Organic Vapor Phase Epitaxy and Chemical Lift-Off of GaN. *Appl. Phys. Lett.* **2007**, *91*, 071120.
22. Lee, T.-H.; Huang, C. H.; Yang, Y. Y.; Suryasindhu, T. Nanoscale Thick Layer Transfer of Hydrogen-Implanted Wafer by Using Polycrystalline Silicon Sacrificial Layer. *Appl. Phys. Lett.* **2007**, *91*, 203119.
23. Singh, S.; Greiner, M. T.; Kruse, P. Robust Inorganic Membranes from Detachable Ultrathin Tantalum Oxide Films. *Nano Lett.* **2007**, *7*, 2676–2683.
24. Lee, W.; Ji, R.; Gösele, U.; Nielsch, K. Fast Fabrication of Long-Range Ordered Porous Alumina Membranes by Hard Anodization. *Nat. Mater.* **2006**, *5*, 741–747.
25. Wehrspohn, R. B. *Ordered Porous Nanostructures and Applications*; Springer: Berlin, 2005.
26. Lu, Q.; Mato, S.; Skeldon, P.; Thompson, G. E.; Masheder, D.; Habazaki, H.; Shimizu, K. Anodic Film Growth on Tantalum in Dilute Phosphoric Acid Solution at 20 and 85 °C. *Electrochim. Acta* **2002**, *47*, 2761–2767.
27. Schwirn, K.; Lee, W.; Hillebrand, R.; Steinhart, M.; Nielsch, K.; Gösele, U. Self-Ordered Anodic Aluminum Oxide Formed by H_2SO_4 Hard Anodization. *ACS Nano* **2008**, *2*, 302–310.
28. Shimizu, K.; Kobayashi, K.; Thompson, G. E.; Skeldon, P.; Wood, G. C. Anodic Oxide Films on Tantalum: Incorporation and Mobilities of Electrolyte-Derived Species. *Philos. Mag. B* **1996**, *73*, 461–485.
29. Shimizu, K.; Kobayashi, K.; Thompson, G. E.; Skeldon, P.; Wood, G. C. The Migration of Fluoride Ions in Growing Anodic Oxide Films on Tantalum. *J. Electrochem. Soc.* **1997**, *144*, 418–423.
30. Sreethawong, T.; Ngamsinlapasathian, S.; Suzuki, Y.; Yoshikawa, S. Nanocrystalline Mesoporous Ta_2O_5-Based Photocatalysts Prepared by Surfactant-Assisted Templating Sol−Gel Process for Photocatalytic H_2 Evolution. *J. Mol. Catal. A* **2005**, *235*, 1–11.
31. Nakayama, Y.; Pauzauskie, P. J.; Radenovic, A.; Onorato, R. M.; Saykally, R. J.; Liphardt, J.; Yang, P. Tunable Nanowire Nonlinear Optical Probe. *Nature* **2007**, *447*, 1098–1102.
32. Zheng, Q.; Zhou, B.; Bai, J.; Li, L.; Jin, Z.; Zhang, J.; Li, J.; Liu, Y.; Cai, W.; Zhu, X. Self-Organized TiO_2 Nanotube Array Sensor for the Determination of Chemical Oxygen Demand. *Adv. Mater.* **2008**, *20*, 1044–1049.
33. Alcala, G.; Skeldon, P.; Thompson, G. E.; Mann, A. B.; Habazaki, H.; Shimizu, K. Mechanical Properties of Amorphous Anodic Alumina and Tantala Films Using Nanoindentation. *Nanotechnology* **2002**, *13*, 451–455.
34. Rizkalla, H.; Wellinghoff, S. T. Inherent Ductility in Amorphous Ta_2O_5 Films. *J. Mater. Sci.* **1984**, *19*, 3895–3907.
35. Lassner, E.; Schubert, W. D. *Tungsten—Properties, Chemistry, Technology of the Element, Alloys, and Chemical Compounds*; Kluwer Academic: New York, 1999.
36. Buslaev, Y. A.; Bochkareva, V. A.; Nikolaev, N. S. The Reaction of Titanium Dioxide with Hydrofluoric Acid. *Russ. Chem. Bull.* **1962**, *11*, 361–364.
37. Meitl, M. A.; Zhu, Z. T.; Kumar, V.; Lee, K. J.; Feng, X.; Huang, Y. Y.; Adesida, I.; Nuzzo, R. G.; Rogers, J. A. Transfer Printing by Kinetic Control of Adhesion to an Elastomeric Stamp. *Nat. Mater.* **2005**, *5*, 33–38.
38. Sun, Y.; Rogers, J. A. Fabricating Semiconductor Nano/Microwires and Transfer Printing Ordered Arrays of Them onto Plastic Substrates. *Nano Lett.* **2004**, *4*, 1953–1959.
39. Vermilyea, D. A. Formation of Anodic Oxide Films on Tantalum in Non-Aqueous Solutions. *Acta Metall. Mater.* **1954**, *2*, 483–486.
40. Macak, J. M.; Tsuchiya, H.; Schmuki, P. High-Aspect-Ratio TiO_2 Nanotubes by Anodization of Titanium. *Angew. Chem., Int. Ed.* **2005**, *44*, 2100–2102.
41. Albu, S. P.; Kim, D.; Schmuki, P. Growth of Aligned TiO_2 Bamboo-Type Nanotubes and Highly Ordered Nanolace. *Angew. Chem., Int. Ed.* **2008**, *47*, 1916–1919.
42. Northen, T. R.; Yanes, O.; Northen, M. T.; Marrinucci, D.; Uritboonthai, W.; Apon, J.; Golledge, S. L.; Nordström, A.; Siuzdak, G. Clathrate Nanostructures for Mass Spectrometry. *Nature* **2007**, *449*, 1033–1036.
43. El-Sayed, H.; Singh, S.; Greiner, M. T.; Kruse, P. Formation of Highly Ordered Arrays of Dimples on Tantalum at the Nanoscale. *Nano Lett.* **2006**, *6*, 2995–2999.
44. Chaneliere, C.; Autran, J. L.; Devine, R. A. B.; Balland, B. Tantalum Pentoxide (Ta_2O_5) Thin Films for Advanced Dielectric Applications. *Mater. Sci. Eng.* **1998**, *R22*, 269–322.
45. Yan, C.; Xue, D. Formation of Nb_2O_5 Nanotube Arrays Through Phase Transformation. *Adv. Mater.* **2008**, *20*, 1055–1058.
46. Müller, K.; Faeh, C.; Diederich, F. Fluorine in Pharmaceuticals: Looking Beyond Intuition. *Science* **2007**, *317*, 1881–1186.
47. Segal, M.; Singh, M.; Rivoire, K.; Voorhis, T. V.; Baldo, M. A. Extrafluorescent Electroluminescence in Organic Light-Emitting Devices. *Nat. Mater.* **2007**, *6*, 374–378.
48. Stair, P. C.; Marshall, C.; Xiong, G.; Feng, H.; Pellin, M. J.; Elam, J. W.; Curtiss, L.; Iton, L.; Kung, H.; Kung, M.; et al. Novel, Uniform Nanostructured Catalytic Membranes. *Top. Catal.* **2006**, *39*, 181–186.